JEECS (Journal of Electrical Engineering and Computer Sciences)
Vol. 11, No. 2, December 2026, pp. 106-121
e-ISSN: 2579-5392 p-ISSN: 2528-0260

Energy Management of Battery–Supercapacitor Hybrid Storage in PV-Integrated DC Microgrids Using Predictive Control

Madhusudan Nyaupane [1], Shanti Tiwari [2], Rajesh M. Pindoriya [3], Jeetendra Chaudhary [4], Asmita Rijal [5]

[1,2,4]Department of Electrical Engineering, Institute of Engineering, Tribhuvan University, Lalitpur, Nepal

[3]Department of Electrical Engineering, Thapar Institute of Engineering & Technology, Patiala, India

[5]Department of Electrical Engineering, Indian Institute of Technology Roorkee, Uttarakhand, India

Article Info

Article history:
Received: 26 February 2026
Revised: 29 April 2026
Accepted: 18 May 2026

Keyword:
Battery Supercapacitor
DC Microgrid
Energy Management Strategy
Photo Voltaic
Predictive Control
Standard Test Conditions

Abstract

This paper addresses the challenge of DC-link voltage instability and control conflicts in Hybrid Energy Storage Systems (HESS) for photovoltaic (PV)-integrated isolated DC microgrids, arising from the inherent variability of Renewable Energy Sources (RES). Existing control strategies often suffer from high computational complexity and inadequate coordination between battery and supercapacitor currents, limiting their effectiveness under dynamic operating conditions. To overcome these limitations, a HESS composed of batteries and supercapacitors is employed, leveraging their complementary characteristics: high energy density and high-power density, respectively. A predictive control strategy is proposed to optimize the current distribution between the battery and supercapacitor using DC-link voltage error and uncompensated power as control inputs. The proposed method is implemented in MATLAB/Simulink and evaluated under varying irradiance conditions (1000 W/m² to 500 W/m² at 25°C) with a 500 W load. The results demonstrate that the proposed approach achieves fast DC-link voltage recovery within approximately 0.1 s, maintains voltage deviation within ±2% of the nominal value, and reduces battery current stress by approximately 30% during transient conditions. Furthermore, the supercapacitor effectively handles rapid transient loads, significantly alleviating battery stress and improving system responsiveness. Additionally, a Bode-plot-based tuning method is employed to refine PI controller parameters, further enhancing energy management and overall system efficiency. These findings highlight the effectiveness of the proposed predictive control strategy as a computationally efficient, dynamically robust solution for the reliable, stable integration of renewable energy into isolated DC microgrids.

Corresponding author:
Rajesh M. Pindoriya, pindoriya.rajesh@thapar.edu

DOI: https://doi.org/10.54732/jeecs.v11i2.1

1. Introduction

Hybrid Energy Storage Systems (HESS), integrating batteries and supercapacitors, have become essential components in isolated DC microgrids with photovoltaic (PV) generation. These systems play a critical role in maintaining power stability, managing fluctuating load conditions, and ensuring a stable DC-link voltage under dynamic operating environments. In such configurations, the battery provides sustained energy for steady-state operation, while the supercapacitor delivers rapid response to transient power variations. This complementary behaviour is fundamental to achieving reliable and efficient system performance [1]. However, in practical implementations, the simultaneous control of battery and

supercapacitor currents during rapid load variations introduces significant challenges. In particular, conflicts between their respective current control loops can degrade system responsiveness and lead to instability, highlighting the need for improved coordinated control strategies [2].

Recent advancements in supercapacitor technologies, including graphene- and carbon nanotube-based electrode materials, have significantly improved their energy density and lifecycle performance, making them more suitable for high-frequency power compensation [3], [4]. At the same time, the rapid growth of renewable energy sources (RES) [5], particularly solar and wind, has increased the complexity of DC microgrid operation due to their intermittent and stochastic nature [6]–[11]. These variations lead to frequent power imbalances, resulting in DC-link voltage fluctuations and reduced system stability [12]–[17]. Therefore, effective coordination between battery and supercapacitor currents is essential to ensure fast voltage regulation and reliable system operation. Several control strategies have been proposed to address HESS coordination. Model Predictive Control (MPC) provides optimized power sharing but suffers from high computational complexity, limiting real-time implementation [18]. Intelligent and optimization-based control techniques have also been explored to improve adaptability and system performance [19], [20], [21]; however, these approaches require significant computational effort for parameter tuning, training, and communication infrastructure. Conventional control approaches, such as sliding mode control and rate-limited control, offer robustness and improved battery lifespan [22]–[24], but they exhibit limitations, such as chattering, insufficient stability analysis, and degraded performance under fast dynamic conditions. Furthermore, coordinated and unified control strategies often fail to effectively resolve conflicts between battery and supercapacitor current control loops, leading to increased DC-link voltage deviations [25]–[30]. energy management, optimization-based control, and distributed coordination frameworks for DC microgrids with HESS [31], [32], [33], [34], [35]. Although these methods improve system efficiency and adaptability, they still suffer from high computational burden, complex implementation, and slower transient response. In particular, dynamic energy management strategies improve power allocation and DC-link voltage regulation under varying load and renewable generation conditions [32]; however, they involve complex control structures and do not explicitly address interactions and conflicts between storage elements. Similarly, hybrid optimisation-based control approaches, such as PSO–GA–LADRC strategies, enhance system stability and power quality but introduce significant computational complexity and are not well suited to fast real-time implementation [33]. Moreover, advanced distributed and coordinated control strategies integrating ANN, droop control, and fuzzy logic improve system stability and adaptability under real-world conditions; however, they rely on multi-layer control architectures and complex coordination mechanisms, which limit their real-time simplicity and practical deployment [21], [34]. In addition, recent comparative studies, such as [36], have evaluated multiple control strategies for hybrid energy storage systems in DC microgrids under dynamic load disturbances, highlighting the importance of coordinated control in improving transient response and DC-link voltage stability. Furthermore, distributed energy storage-based coordinated control strategies, such as [35], improve power sharing and voltage regulation using optimization techniques; however, they rely on complex scheduling algorithms and do not explicitly address fast dynamic response and control conflict issues. Therefore, the key research gap lies in the lack of a computationally efficient control strategy that can simultaneously (i) eliminate control conflicts between battery and supercapacitor currents, (ii) ensure fast DC-link voltage regulation under dynamic conditions, and (iii) be implemented in real time without complex optimization, training, or multi-layer control structures.

To address this gap, this paper proposes a simplified predictive control-based energy management strategy for a PV-integrated DC microgrid with HESS. The proposed method directly computes the duty cycle using a predictive term, significantly reducing computational complexity compared to conventional MPC and optimization-based approaches. Furthermore, by incorporating DC-link voltage error and uncompensated battery power into the supercapacitor control loop, the proposed strategy effectively eliminates controller conflicts, enhances transient response, and ensures rapid DC-link voltage recovery. Consequently, the proposed method improves system stability, reduces battery stress, and enables practical real-time implementation.

Table 1 provides a comprehensive comparison of existing HESS control strategies, integrating qualitative metrics (complexity, response speed, and real-time feasibility) and quantitative performance indicators (settling time, overshoot, and DC-link voltage ripple). It is evident that conventional and optimization-based methods, such as MPC and PSO-based approaches, achieve acceptable voltage regulation but suffer from high computational complexity and slower transient response, limiting their real-time applicability. Similarly, intelligent and hybrid control techniques improve adaptability but introduce multi-layer complexity and implementation challenges.

Table 1. AC Microgrid power

Ref.	Control Technique	Compl-exity	Response	Real-Time	Settling Time (ms)	Overs hoot (%)	Ripple (%)	Key Contribution	Research Gap
[18]	MPC	High	Medium	Low	25–40	6–10	2–3	Optimal power sharing with constraints	High computatio nal burden
[19]	Fuzzy Logic	Medium	Medium	Medium	30–50	8–12	3–4	Adaptive power allocation	Weak stability analysis
[22]	Rate Limit	Low	Slow	High	60–100	10–15	4–6	Battery lifespan improvement	Poor dynamic response
[23], [24]	Sliding Mode	Medium	Fast	Medium	15–30	5–8	2–3	Robust under disturbances	Chattering; conflicts
[25]	Unified Control	Medium	Medium	Medium	35–60	7–12	3–5	SOC-based coordination	Voltage deviation; conflicts
[31]	EMS	Med–High	Medium	Medium	30–55	6–10	3–4	Coordinated HESS operation	Complex; slower response
[20]	Optimizatio n-Based	High	Medium	Low	40–70	8–13	4–5	Improved voltage stability	High complexity
[32]	Dynamic EMS	High	Medium	Low	35–65	7–12	3–5	Adaptive power sharing	No conflict handling
[33]	PSO-GA-LADRC	Very High	Slow–Med	Low	50–90	6–10	3–4	Enhanced stability & PQ	Not real-time feasible
[21]	ANN-Based	High	Medium	Low–Med	25–45	5–9	2–3	Adaptive distributed control	Requires communica tion
[34]	Droop + Fuzzy	High	Medium	Low–Med	30–60	6–11	3–4	Multi-layer coordinated control	High complexity
[36]	Comparativ e Study	—	Medium	—	30–70	6–12	3–5	Performance benchmarking	No control design
[35]	PSO-Based Control	High	Medium	Low	45–80	7–12	4–6	Optimized scheduling & sharing	Optimizatio n-dependent
Propo sed	Predictive EMS	Low	Fast	High	8–15	1–3	<1.5	Direct duty control; conflict-free	Low complexity, real-time capable

In contrast, the proposed predictive EMS demonstrates superior overall performance, achieving the fastest settling time (8–15 ms), minimal overshoot (1–3%), and lowest DC-link voltage ripple (<1.5%), while maintaining low computational complexity and high real-time feasibility, effectively addressing the limitations of existing methods. The performance metrics presented in Table 1 are defined as follows. Complexity represents the computational burden and algorithmic structure of each control method, categorized from Low to Very High. Transient response indicates the speed of DC-link voltage recovery following disturbances and is classified as Slow, Medium, or Fast. Real-time feasibility reflects the suitability of the control strategy for implementation in embedded or real-time systems, categorized as Low, Medium, or High. Additionally, quantitative performance indicators such as settling time, overshoot, and DC-link voltage ripple are used to evaluate dynamic response and voltage regulation capability.

The organization of this article is as follows: Section II presents the overall system design and modelling methodology. Section III includes modelling of PV systems with a battery and a supercapacitor as energy storage. Section IV gives an energy management strategy. Section V presents detailed simulation results for HESS, and Section VI concludes the paper.

2. Research Methodology

2.1. System Design and Modeling Methodology

2.1.1 Solar PV Modelling

The design and modelling of a Solar Photovoltaic (SPV) system involve several crucial steps, including modelling the PV system itself, implementing an efficient Maximum Power Point Tracking (MPPT)

algorithm, and using optimization tools to improve overall system performance. One important aspect of SPV system modelling is the creation of a test cell to measure the values of Isc and Voc, which can then be used to accurately model the system's behavior. Additionally, modelling the PV system and developing a new MPPT system are essential components of the design process. Figure 4(a) represents the electrical model of a PV cell consisting of a photocurrent and a diode describing the properties of the semiconductor [37]. A series resistance R_s represents an internal resistance, and a parallel resistance Rp shows a leakage current [38]. The mathematical equation expressing the charging current can be given as [33]: Based on Eq. (1), we see that the physical behaviour of the PV cell is also related to temperature and solar radiation [37], so for a given temperature of 25°C, and variable radiation. The I-V and P-V curves are generated as shown in Figure 1.

$$I = I_{ph} - I_s\left[e^{\left(\frac{qv+IR_s}{kT_cA}\right)} - 1\right] - \left(\frac{V+IR_s}{R_p}\right) \quad (1)$$

where, I_s is the saturation current, I_{ph} is the solar induced current, q is the elementary charge of the electron, A is the ideality factor (the emission coefficient for the diode) of the diode, I is the output current of PV, V is the output voltage of PV, R_s is the series resistance, R_p is the shunt resistance, K is the boltzmann's constant, and T_c is the temperature at STC.

The Figure 1 shows the I-V (current-voltage) and P-V (power-voltage) characteristics of a photovoltaic (PV) system under varying irradiance levels and constant temperature. The I-V Characteristics (Top Plot), represent the relationship between current (I) and voltage (V) for different irradiance levels (0.25 kW/m^2 to 1 kW/m^2). As the irradiance increases, the short-circuit current (I_{sc}) increases proportionally. This is because more sunlight generates a higher photoelectric current. The open-circuit voltage (V_{oc}) increases slightly with higher irradiance but remains nearly constant compared to the current. The P-V Characteristics (Bottom Plot), represent the power (P) output as a function of voltage (V) for varying irradiance levels. The peak power increases significantly with higher irradiance. The maximum power point (MPP) shifts slightly with changes in irradiance, leading to changes in voltage and current. At low irradiance (e.g., 0.25 kW/m^2), both current and power are significantly reduced.

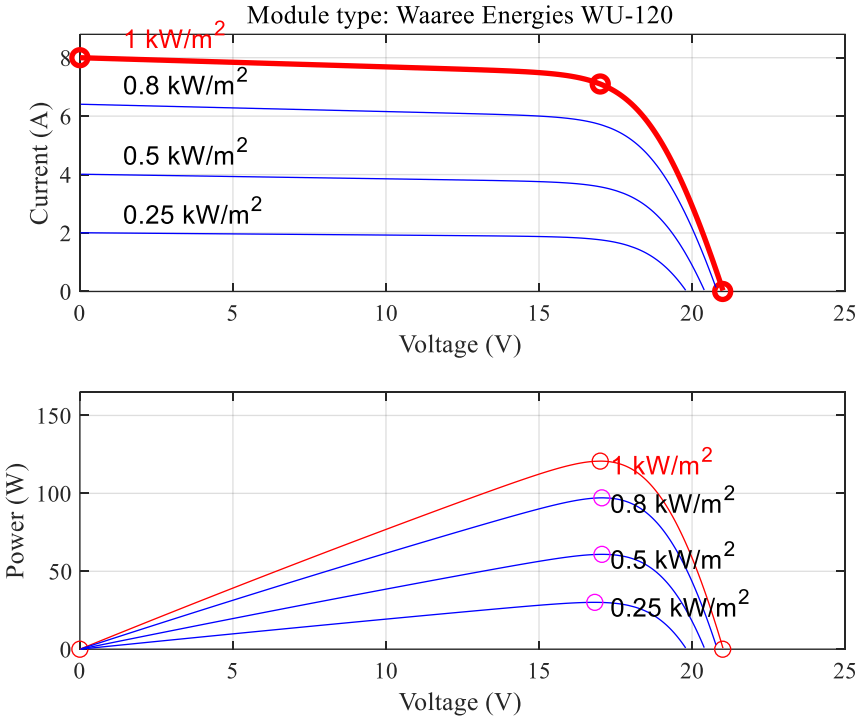

Figure 1. Characteristics of PV with varying irradiances and temperatures.

2.1.2 Battery Modelling

The model is shown in Figure 2 (b), it consists of a voltage source corresponding to the open circuit voltage source E_0 in series with an equivalent internal resistance R_s [39].
The terminal voltage of the battery is given by (2):

$$V_B = E_0 - I_B . R_B \quad (2)$$

Where, E_0 = EMF of cell, I_B = Current through battery and R_B = Battery resistance

The state of charge (SOC) of the battery is also defined by [40]:

$$SOC = 1 - \frac{Q_d}{C_b} \quad (3)$$

Where, Q_d is the discharged capacity and C_b is the nominal capacity of the battery. This model captures the essential dynamic characteristics of the battery during charging and discharging.

2.1.3 Supercapacitor Modelling

This is a simple electrical circuit model consisting of a resistor R_{sc} and a capacitor C_{sc} in series (Figure 4(c)). This model is commonly used for the study of energy systems. The expression for the SC voltage V_{SC} is given by (8) [41].

$$V_{SC} = \frac{Q_{SC}}{C_{SC}} - R_{SC} I_{SC} \quad (4)$$

Due to its high-power density and fast response, the supercapacitor handles transient variations in load power, thereby relieving the battery from the burden of instantaneous current surges.

2.1.3 DC-DC Converter Modelling

Choppers are static DC-DC converters that provide a variable DC voltage from a fixed DC voltage. This energy conversion is carried out at a high frequency, "chopping" characterized by high efficiency. The boost converters are used after the PV and fed to the DC bus.

The output voltage of the Boost converter is given as:

$$V_{dc,pv} = \frac{V_{pv}}{1-D} \quad (5)$$

where D = duty cycle

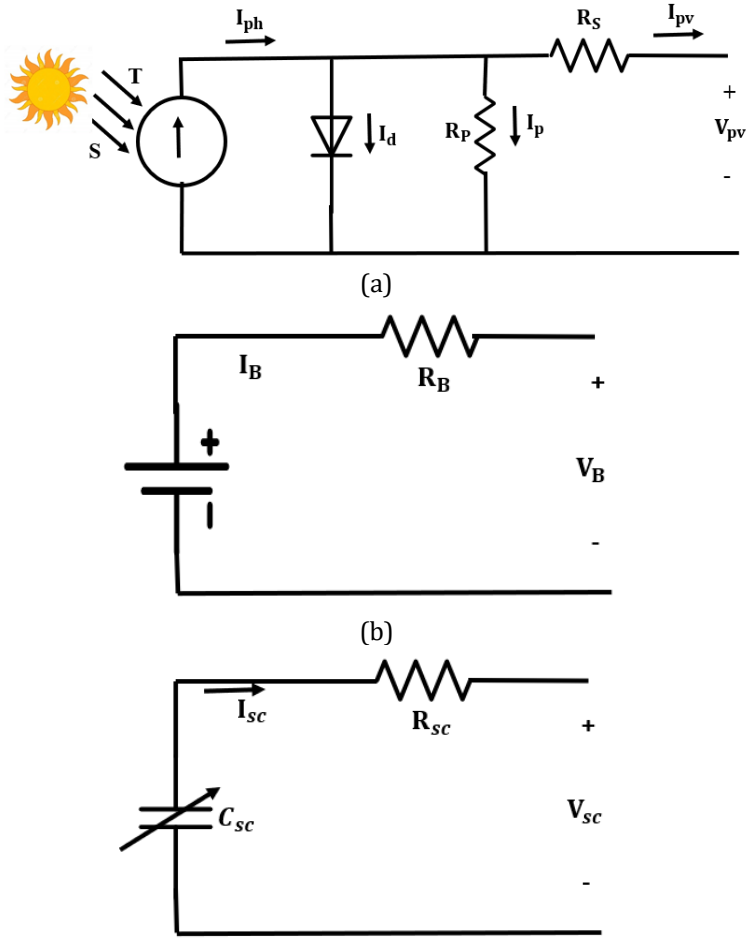

Figure 2. Electrical model: (a) PV cell; (b) Battery; (c) Supercapacitor.

The proposed system contains two transistor switches; the method of controlling them determines the bidirectional converter's operating mode (buck or boost) for battery- and supercapacitor-type converters. During charging, the bidirectional converter operates as a boost converter in which the output voltage is given by,

$$V_{dc,B} = \frac{V_B}{1-D} \quad (6)$$
$$V_{dc,B} = D\,V_B \quad (7)$$
$$V_{dc,sc} = \frac{V_{sc}}{1-D} \quad (8)$$
$$V_{dc,SC} = D\,V_{SC} \quad (9)$$

The bidirectional converter allows charging and discharging of the battery based on the system's power balance, enabling smooth transitions between energy surplus and deficit conditions.

2.2. Modelling of PV system with HESS

The proposed stand-alone photovoltaic system with hybrid storage consists of a PV generator connected to a DC bus via a DC-DC boost converter, and a group of lithium-ion batteries as a long-term storage system used in case of overconsumption or under-supply, based on the characteristics of fast charging at different temperatures, and The extended life cycle of this type of rechargeable battery according to the proposed model represents a more suitable option, compared to the lead-acid battery [42], [43] .and a set of supercapacitors to cope with rapid transitions in power demand, each ESS (Electrical Energy Storage) is connected to the DC bus via a DC-DC buck-boost converter, loads, a three-phase inverter connected to the DC bus is used to power the load and control systems [44]. As shown in Figure 1. The PV system is affected by various weather conditions, including irradiance. Therefore, MPPT control is used to extract the maximum power from the PV via DC/DC amplification for proper operation of the PV system, which is achieved using the Perturbation and Observation (P&O) method. Power transfer between these components is via conventional energy. Management system. The proposed model is developed and simulated in MATLAB/Simulink using mathematical analysis, and the average model is shown in Figure 3.

The semi-active hybrid energy storage system integrates a photovoltaic (PV) system, a battery, and a supercapacitor (SC), all connected to a common DC link via bidirectional DC-DC converters. The PV system converts solar energy into electrical energy, which is connected to the DC link via a DC-DC converter that regulates voltage and current; the converter's output current is denoted as i_{pv}. The DC link acts as a shared bus for energy transfer among the PV system, battery, and supercapacitor, stabilized by its total capacitance C_{dc} and load resistance R_{dc}.

The battery and supercapacitor are connected to the DC link via bidirectional DC-DC converters, enabling energy flow in both directions for charging and discharging, with their respective currents represented as i_b and i_{sc}. Filter inductors (L_{pv}, L_b, L_{sc}) are used to smooth the output currents of the PV, battery, and supercapacitor converters. System voltages include v_{pv} (PV), v_{bat} (battery), v_{sc} (SC), and v_{dc} (DC link), which must remain within specific limits for optimal operation.

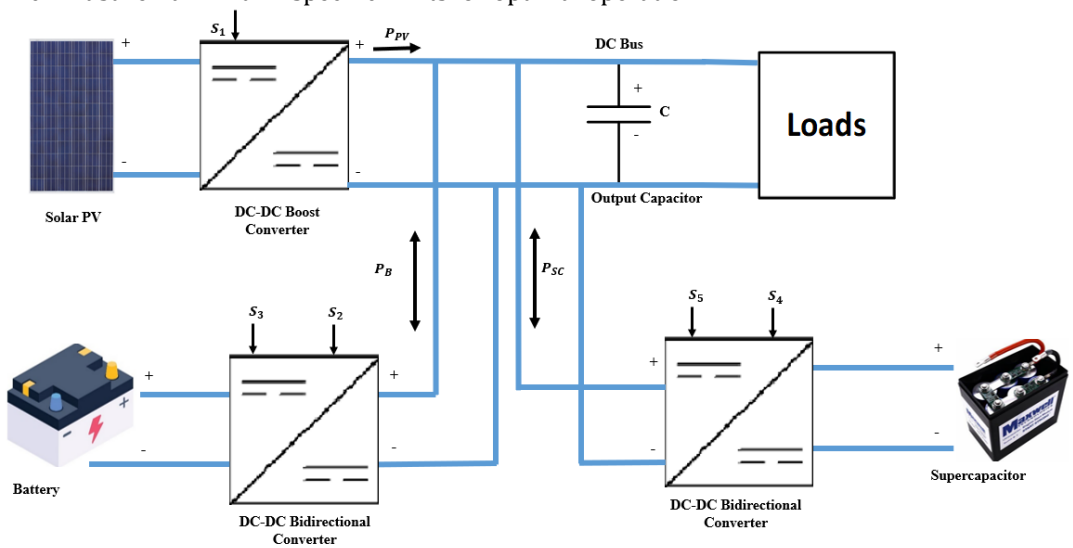

Figure 3. Block diagram of PV systems with Hybrid energy storage

Control switches S_1-S4 dynamically regulate energy flow based on system demand, ensuring efficient distribution. This architecture enables efficient energy harvesting, storage, and sharing, with precise control ensuring the system can adapt dynamically to changing load conditions. The control schemes for the overall system are as in Figure 4.

Super capacitor inner current loop transfer function is defined by,

$$G_{id\_SC} = \frac{i_{SC}}{d_{SC}} = \frac{V_{DC}\,CS + 2\frac{V_{DC}}{R}}{L_{SC}\,CS^2 + \frac{L_{SC}}{R} + (1-d_{SC})^2} \quad (10)$$

$$G_{pi,SC} = K_{p,SC} + \frac{K_{i,SC}}{S} \quad (11)$$

Battery inner current loop transfer function

$$G_{id\_B} = \frac{i_B}{d_B} = \frac{V_{DC}\,CS + 2\frac{V_{DC}}{R}}{L_B\,CS^2 + \frac{L_B}{R} + (1-d_B)^2} \quad (12)$$

$$G_{pi,B} = K_{p,B} + \frac{K_{i,B}}{S} \quad (13)$$

Outer voltage loop transfer function

$$G_{vi\_v} = \frac{V_{DC}}{i_{SC}} = \frac{R\,(1-d_{SC})\,.\,(1-\frac{L_{SC}}{R\,(1-d_{SC})^2}}{2+RCS} \quad (14)$$

$$G_{pi,v} = K_{p,v} + \frac{K_{i,v}}{S} \quad (15)$$

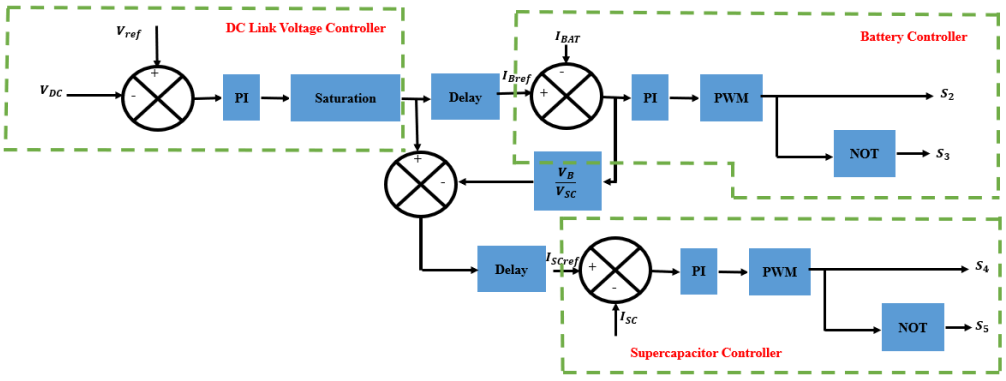

(a)

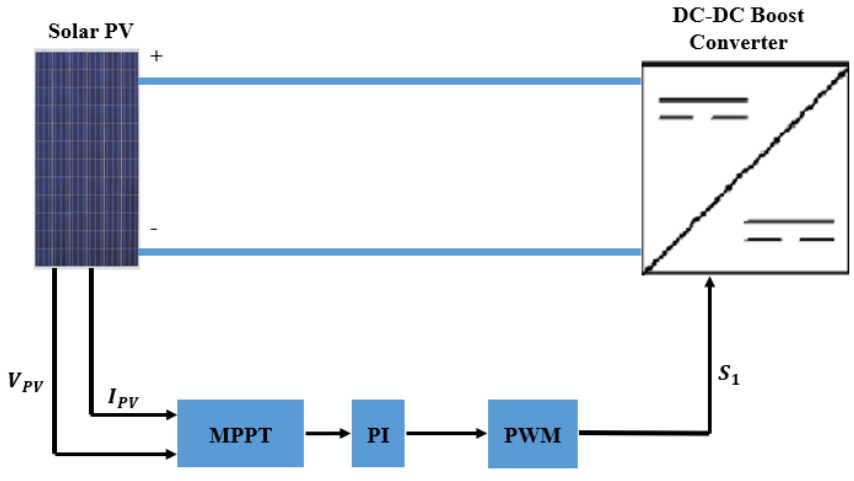

(b)

Figure 4. Control system: (a) Battery- SC Control; (b) PV control

Table 2. Controller Parameters.

Parameters	PV converter	Battery converter	Supercapacitor controller	DC link Voltage Controller
K_p	0.3	0.05	0.48	1.477
K_i	0.3	0.63	14803	3077

Figure 4(a) illustrates the hierarchical control of the HESS, which distributes power between the battery and supercapacitor to maintain DC-link voltage stability and protect the battery from high-frequency transients. The total power imbalance is decomposed into low- and high-frequency components, with the battery handling slow variations and the supercapacitor responding to rapid fluctuations. Predictive PI-based current controllers regulate the charging and discharging of each storage unit based on state-of-charge (SOC) limits, ensuring safe operation. This coordinated approach allows the supercapacitor to quickly compensate for sudden load or irradiance changes while the battery restores energy more gradually, resulting in smoother DC voltage and reduced stress on the battery. Also, the control strategy depicted in Figure primarily focuses on regulating the DC-link voltage of the PV–DC bus while ensuring maximum power extraction from the PV array. The PV array produces a variable DC voltage depending on solar irradiance and temperature, and an MPPT algorithm, such as Perturb & Observe, continuously adjusts the reference current to maintain operation at the Maximum Power Point. This reference guides the boost converter, whose duty cycle is modulated by a voltage and current control loop to maintain the DC-link voltage at its desired reference. When PV generation exceeds load demand, the surplus energy charges the HESS, and when generation is insufficient, the HESS discharges to stabilize the voltage. The values of K_p and K_i for different controllers are calculated and given in Table 2.

2.3. Energy Management Strategy

The proposed predictive control-based EMS dynamically regulates the power balance between the PV system, the battery, and the supercapacitor in response to instantaneous generation and load demand. The main control objective is to maintain the DC-link voltage V_{dc} close to its reference $V_{dc,ref}$ while minimizing battery current stress. The total power balance of the DC microgrid is,

$$P_{pv} + P_b + P_{sc} = P_L \quad (16)$$

by predicting the next-step states of V_{dc}, I_{bat} and I_{sc}. The controller determines optimal duty ratios for the DC–DC converters.

The flowchart presents a detailed Energy Management Strategy (EMS) for a HESS composed of a PV array, a battery, and an SC. The control logic is designed to ensure uninterrupted power delivery to the load while optimizing solar energy use and safeguarding the energy storage components from overcharging or excessive discharge. At each control cycle, the algorithm begins by reading the real-time power outputs of the PV system, the battery, and the supercapacitor, along with the load power demand and the state of charge (SOC) of both the battery and the SC. It then calculates the power error, defined as the difference between the PV power and the load power. This error determines whether the system is experiencing a power surplus (PV generation exceeds load demand) or a deficit (PV generation is insufficient). In the case of a power deficit, when the load demand exceeds the available PV power, the controller checks whether the PV system is supplying at least 70% of the load demand. This 70% threshold ensures that the PV plays a major role in supplying the load, making it reasonable to include storage components for balancing. If the PV meets this condition, the system first attempts to discharge the supercapacitor, provided its SOC is above the minimum threshold. If the supercapacitor alone cannot make up the deficit or if its SOC is too low, the controller checks the battery's SOC and discharges it if it is adequately charged. In scenarios where neither the SC nor the battery can meet the demand individually, the system uses both devices in combination to support the load. However, if none of the energy storage components has sufficient charge, the system disconnects the load to prevent damage to the storage devices. When there is a power surplus, meaning the PV generation exceeds the load demand, the controller again verifies whether the PV is supplying at least 70% of the load. If so, it then manages the excess energy intelligently. The supercapacitor is prioritized for charging when its SOC is below the upper threshold, given its fast response and ability to handle rapid energy bursts. If the SC is already fully charged, the battery is next in line to store the excess energy, provided its SOC is within the safe charging range. If both the SC and the battery are fully charged, the system disables the PV array's Maximum Power Point Tracking (MPPT) algorithm to limit its output and prevent overvoltage or system instability. This control architecture follows a hierarchical, protective logic, giving precedence to the supercapacitor for handling rapid, transient power fluctuations and to the battery for managing longer-term energy requirements. The use of SOC thresholds ensures the longevity and safe operation of the energy storage units. The 70% PV contribution rule acts as a stability filter, ensuring that switching between operating modes happens only when the PV system is playing a dominant role. Overall, the strategy is designed to maximize solar energy use, ensure continuous load supply, minimize battery degradation, and enhance the HESS's efficiency and reliability under both steady and dynamic conditions. The algorithm implemented for the PMS is shown in the flowchart in Figure 5. The proposed predictive control-based Energy Management Strategy (EMS) is validated using MATLAB/Simulink under realistic operating conditions of a PV-integrated DC microgrid with hybrid energy storage.

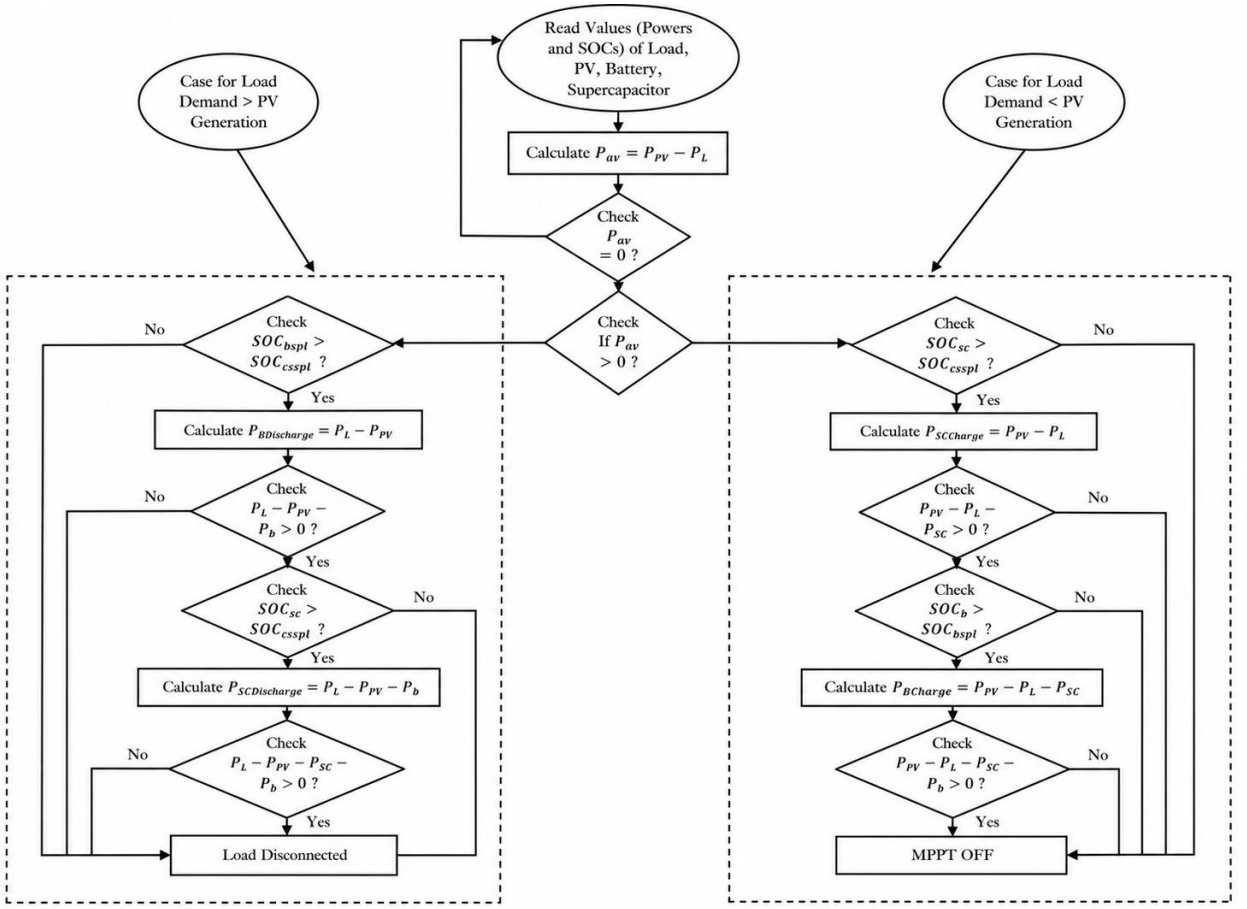

Figure 5. Flowchart of EMS.

The evaluation includes steady-state and dynamic analyses, in which irradiance is varied from 1000 W/m^2 to 500 W/m^2 at 25°C, with a 500 W load, to emulate practical scenarios. Performance is assessed based on DC-link voltage regulation, settling time, overshoot, voltage ripple, and reduced battery stress. Scenario-based testing is conducted for both power deficit (load > PV) and surplus (PV > load) conditions, ensuring proper coordination of battery and supercapacitor operations under SOC constraints. Additionally, comparison with existing methods (Table 1) confirms improved transient response, reduced complexity, and enhanced real-time feasibility, demonstrating the robustness and effectiveness of the proposed EMS.

3. Results and Discussions

The simulation is implemented in MATLAB/ Simulink. The PV power generation is 960 watts at STC (1000 W/m^2 irradiance and 25°C), and a load of 500 Watts is used. During the simulation, the temperature is fixed, but the system is tested at varying irradiances of 1000 W/m2 at 25°C and 500 W/m^2 at 25°C. The response of the battery is shown in Figure 6. The battery voltage response is shown in Figure 6 (a). The battery voltage remains steady, indicating that the battery operates within its nominal voltage range. There are slight dips or fluctuations, possibly corresponding to changes in the load or operating conditions. After the transient event (around 12 seconds), the voltage stabilizes again, suggesting recovery from the disturbance. The battery current response is shown in Figure 6 (b). The current waveform exhibits significant changes during the simulation. It shows spikes or steps that correspond to load demands or switching events. Initially, the current is steady, but changes in the middle of the plot indicate a sudden increase or decrease in load. The battery SoC response is shown in Figure 6 (c). The SoC exhibits a gradual decline, as expected during battery discharge. The linear slope in SoC indicates constant energy consumption initially. The battery power response is shown in Figure 6 (d). The power plot represents the product of battery voltage and current. It shows dynamic changes in response to load variations. The power initially remains at a certain level, rises with increasing load, and then reduces significantly after the transient event.

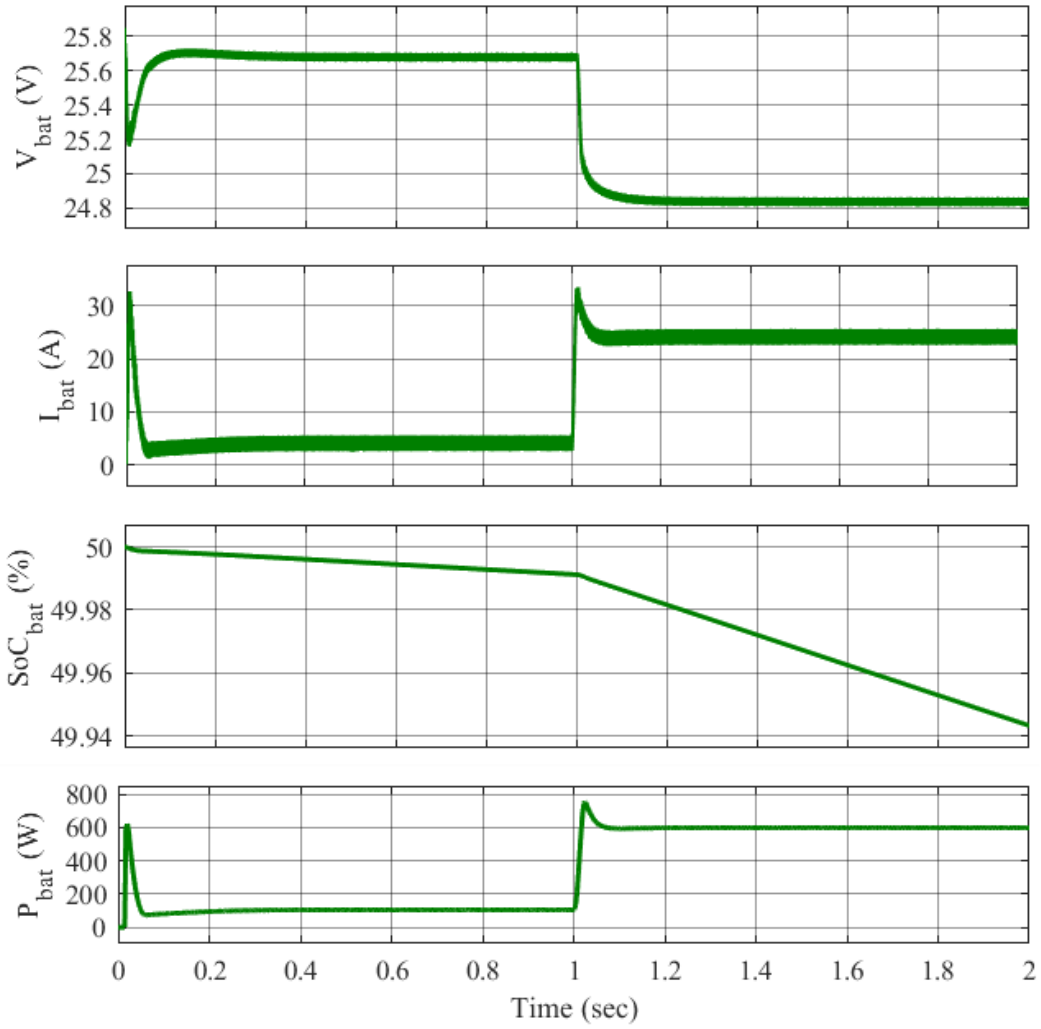

Figure 6. Battery response: (a) Voltage, (b) Current, (c) SOC and (d) Power.

The response of the super capacitor is shown in Figure 7. The voltage response is shown in Figure 7 (a). The voltage starts at its nominal value (~31.8 V) and remains stable during the initial phase. Around 1 second, a sharp drop is observed, likely caused by a sudden increase in load or current demand. After this transient, the voltage stabilizes again, indicating the supercapacitor's ability to recover. The current response is shown in Figure 7 (b). The current exhibits dynamic behaviour with small fluctuations due to load changes. A significant spike occurs around 1 second, corresponding to the transient increase in load. Post-transient, the current returns to its steady-state value, consistent with a stabilized load. The SoC response is shown in Figure 7 (c). The SOC shows a gradual decline, representing energy discharge from the supercapacitor during normal operation. A sudden dip around 1 second corresponds to the high current demand observed in subplot Figure 7 (b**)**. After the event, the SOC decreases more slowly, indicating a return to normal operation with lower power demand. The power response is shown in Figure 7 (d). Power starts at low values and fluctuates slightly under initial steady conditions. Around 1 second, a large spike is observed, representing a significant energy demand from the supercapacitor. After the transient, the power stabilizes at a lower level, reflecting the steady-state condition of the system.

The Figure (8) shows the graph for the solar voltage, solar current and solar power generated to supply the 500 watts of load. The response of the solar voltage is shown in Figure 8(a). The voltage exhibits small fluctuations due to the nature of solar PV systems and their dependence on environmental factors such as irradiance and temperature. Around the 10-second mark, a sharp dip occurs, likely due to a transient event, such as a load increase or a reduction in irradiance. After this event, the voltage stabilizes, indicating the PV system's capability to recover and adapt to new operating conditions. The response of the solar current is shown in Figure 8 (b). The current initially fluctuates slightly, reflecting the dynamic nature of the PV system in response to environmental inputs or load variations. The response of solar power is shown in Figure 8 (c). The power output rises sharply during the initial phase, then stabilises as the system reaches its

maximum power point under steady conditions. At around 10 seconds, there is a sharp drop in power output, which aligns with the observed reductions in voltage and current.

Figure 9 illustrates the power dynamics in a hybrid energy system integrating Solar PV, Load, Battery, and Supercapacitor (SC) under transient and steady-state conditions. Figure 9(a) shows the solar PV system starts from zero and ramps up to ~1000 W in steady state. Around 1 second, a sharp dip occurs, likely due to reduced irradiance or load redistribution. After stabilization, the PV delivers power within operational limits. Figure 9(b) shows that the load demand remains ~600 W, with minor fluctuations lasting ~1 second, indicating transient balancing by the energy management system.

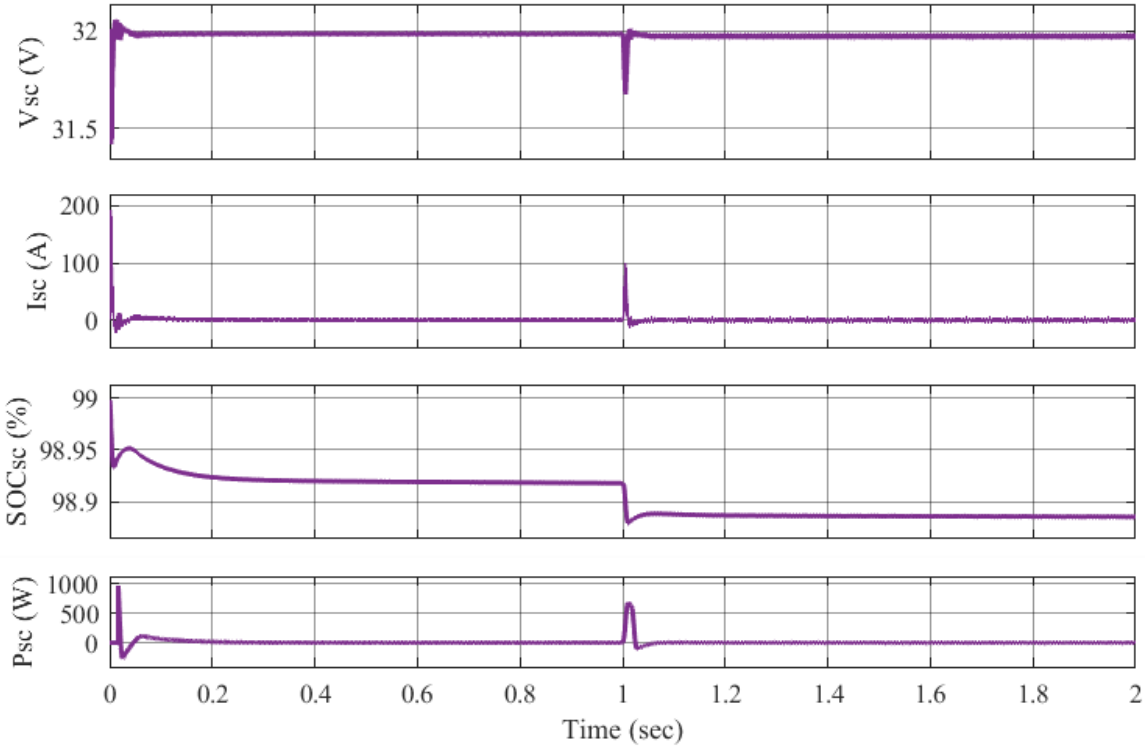

Figure 7. Super Capacitor Response: (a) Voltage, (b) Current, (c) SoC and (d) Power.

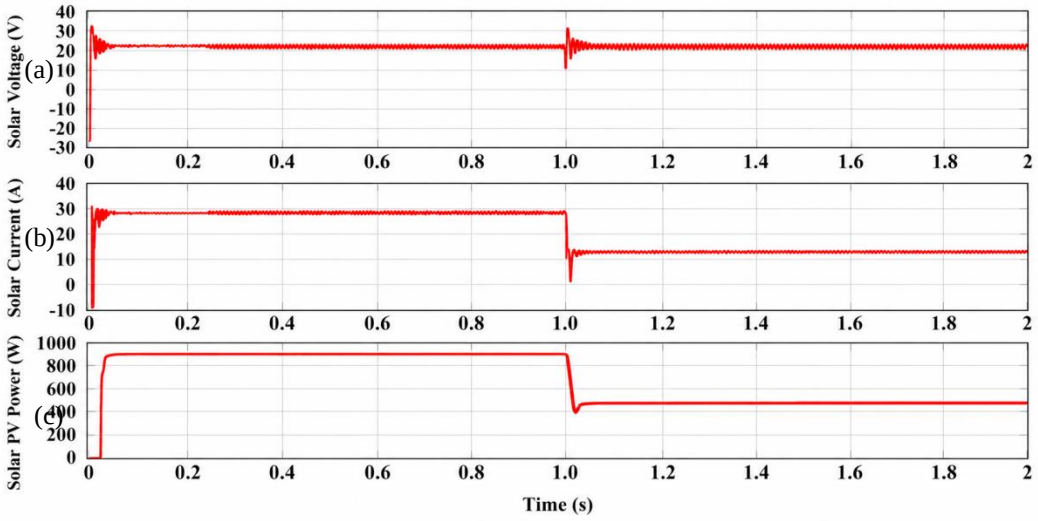

Figure 8. Response of Solar PV: (a) Voltage; (b) Current and(c) Power.

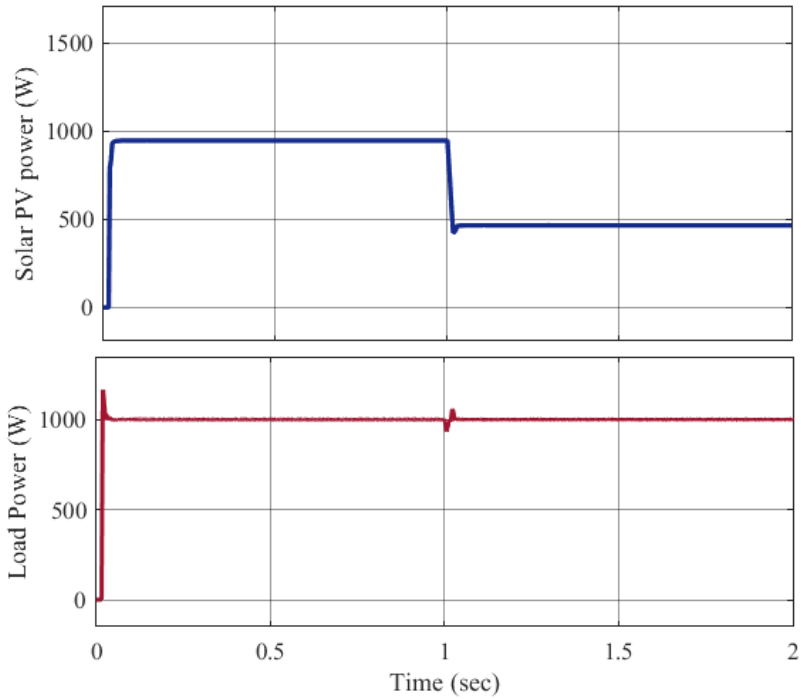

Figure 9. Power response of hybrid source: (a) PV Power, and (b) Load Power.

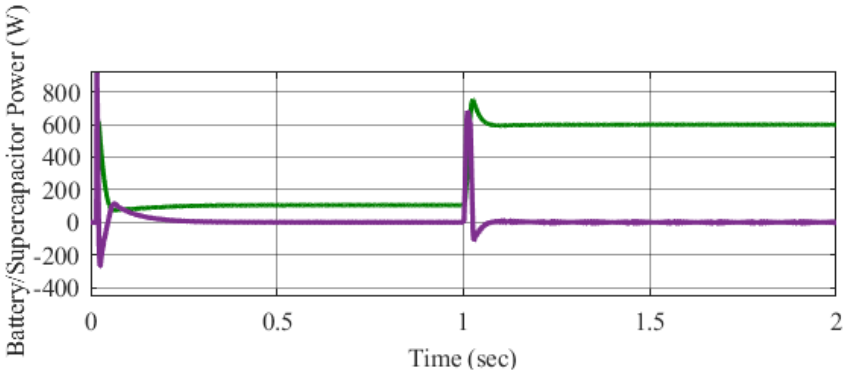

Figure 10. Power response of battery and supercapacitor.

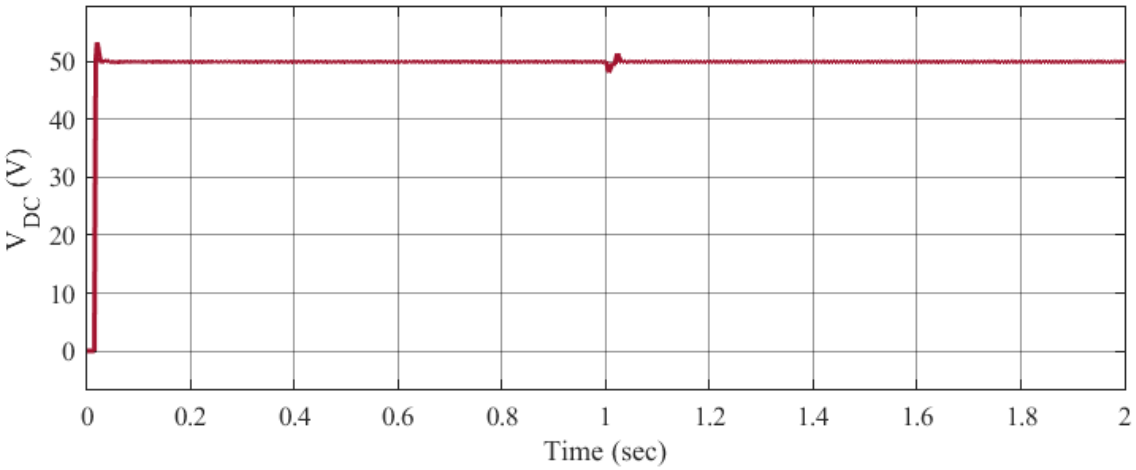

Figure 11. DC link voltage.

Table 3. Extracted Quantitative Performance Results of Proposed EMS

Category	Parameter	0–1 s (1000 W/m^2)	1–2 s (500 W/m^2)	Key Observation
DC-Link	(V_{DC}) (V)	50–52 (initial overshoot), settles ≈ 50	49–50	Maintained within ±2%
	Settling Time (ms)	≈ 10 ms	≈ 12–15 ms	Very fast stabilization
	Overshoot (%)	≈ 2–3%	≈ 2%	Minimal deviation
PV System	PV Voltage (V)	≈ 22–25	≈ 20–22	Slight drop with irradiance
	PV Current (A)	≈ 30	≈ 15	Proportional reduction
	PV Power (W)	≈ 900–950 W	≈ 450–500 W	Accurate MPPT tracking
Load	Load Power (W)	≈ 1000 W	≈ 1000 W	Fully supplied
Battery	(V_{bat}) (V)	≈ 25.6–25.7	≈ 24.8–25	Stable operation
	(I_{bat}) (A)	≈ 3–5 A	≈ 22–25 A (peak ~30 A)	Controlled current rise
	SOC (%)	≈ 50 → 49.99	≈ 49.99 → 49.94	Smooth discharge
	(P_{bat}) (W)	≈ 100–150 W	≈ 600–700 W	Supplies deficit power
Supercapacitor	(V_{sc}) (V)	≈ 31.8–32	≈ 31.7–32	Stable voltage
	(I_{sc}) (A)	≈ 0 (steady)	Peak ≈ 80–100 A	Handles transient spike
	SOC (%)	≈ 98.95 → 98.92	≈ 98.92 → 98.88	Slight drop
	(P_{sc}) (W)	≈ 0–50 W	Peak ≈ 600–800 W	Absorbs fast dynamics
Power Sharing	Battery vs SC	Battery dominant (steady)	SC dominant (transient)	Effective coordination
Dynamic Response	Recovery Time	—	≈ 0.1 s	Fast disturbance rejection
System Stability	Oscillations	None	None	Stable response

Figure 10 shows the battery & Supercapacitor Power. The battery initially supplies significant power, then stabilises after the transient. The supercapacitor provides a short-term surge, stabilizing the system before its contribution diminishes. Figure 11 shows the DC link voltage of a power system over time. During Initial Transient (0–0.1s), the voltage rapidly rises to ~50V, indicating capacitor charging. In Steady-State Operation (0.1–1s), it stabilizes around 50V with minimal ripple. At Disturbance (~1s), a brief dip occurs due to a load change but quickly recovers. Post-Disturbance (1–2s), stability is restored. The system effectively regulates voltage, ensuring minimal ripples and quick disturbance recovery.

The results presented in Table 3, extracted directly from the simulation figures, confirm the superior performance of the proposed predictive EMS under both steady-state and transient conditions. The DC-link voltage is tightly regulated at 50 V, with a maximum overshoot of approximately 2–3% and a fast-settling time of about 10–15 ms, ensuring stable operation. Under irradiance variation from 1000 W/m^2 to 500 W/m^2 at 1 s, the PV power accurately tracks the change from approximately 950 W to 500 W, demonstrating effective MPPT operation. During this transition, the supercapacitor delivers a high transient current (up to ~100 A) and power (~800 W), rapidly compensating for sudden power mismatch, while the battery provides sustained support with controlled current increase (up to ~25 A). This coordinated behaviour significantly reduces battery stress and prevents abrupt current spikes. The battery SOC shows a smooth and minimal decrease (50% to ~49.94%), confirming efficient energy utilization. Furthermore, the system exhibits fast recovery (~0.1 s) with no observable oscillations, and the load demand (~1000 W) is continuously satisfied. These results clearly demonstrate that the proposed EMS achieves excellent dynamic response, effective power sharing, and enhanced system stability, making it a robust and practical solution for PV-integrated DC microgrid applications.

4. Conclusion

This paper addresses the critical challenges of integrating Renewable Energy Sources (RES), particularly photovoltaic (PV) systems, into isolated DC grids. A Hybrid Energy Storage System (HESS) composed of batteries and supercapacitors was proposed to enhance grid stability and energy management. The predictive control strategy developed in this work demonstrated its effectiveness in balancing the

current distribution between the battery and supercapacitor. Simulations in MATLAB/Simulink validated the approach, revealing faster voltage restoration, reduced battery stress, and improved grid responsiveness under various operational scenarios. Furthermore, the application of a bode plot tuning method for PI controllers optimized system performance, ensuring effective energy management and enhanced overall efficiency. Key findings highlight the supercapacitor's ability to manage rapid transient loads, significantly alleviating battery wear and extending its operational lifespan. These results underscore the potential of advanced control strategies to address integration challenges in isolated DC grids, thereby enabling the stable and efficient utilization of renewable energy.

Future work could explore real-world implementations of the proposed strategy, evaluate its scalability, and investigate its applicability in hybrid AC/DC grids. By advancing HESS control techniques, this research supports the broader adoption of renewable energy and fosters the development of resilient, sustainable power systems.

Declarations

All authors declare that they have no conflicts of interest.

Acknowledgement

All authors declare that they have no funding support from anyone.

Author's Contribution Declaration

Madhusudan Nyaupane, Shanti Tiwari and Rajesh M. Pindoriya wrote the main manuscript and developed the control algorithm. Jeetendra Chaudhary, and Asmita Rijal prepared simulation, figures, tables, and proofreading.

References

[1] G. Wang *et al.*, "A review of power electronics for grid connection of utility-scale battery energy storage systems," *IEEE Transactions on Sustainable Energy*, vol. 7, no. 4, pp. 1778–1790, Oct. 2016, doi: 10.1109/TSTE.2016.2586941.

[2] X. Wang, D. Yu, S. Le Blond, Z. Zhao, and P. Wilson, "A novel controller of a battery-supercapacitor hybrid energy storage system for domestic applications," *Energy and Buildings*, vol. 141, pp. 167–174, Apr. 2017, doi: 10.1016/J.ENBUILD.2017.02.041.

[3] D. J. Pandya *et al.*, "Supercapacitors: Review of materials and fabrication methods," *Materials Today: Proceedings*, Nov. 2023, doi: 10.1016/J.MATPR.2023.10.148.

[4] D. P. Chatterjee and A. K. Nandi, "A review on the recent advances in hybrid supercapacitors," *Journal of Materials Chemistry A*, vol. 9, no. 29, pp. 15880–15918, Jul. 2021, doi: 10.1039/D1TA02505H.

[5] A. M. Adeyinka, O. C. Esan, A. O. Ijaola, and P. K. Farayibi, "Advancements in hybrid energy storage systems for enhancing renewable energy-to-grid integration," *Sustainable Energy Research 2024 11:1*, vol. 11, no. 1, pp. 26-, 2024, doi: 10.1186/S40807-024-00120-4.

[6] Y. Chen, Y. Chen, L. Zhang, and Z. Li, "Revealing the role of renewable energy consumption and digitalization in energy-related greenhouse gas emissions—Evidence from the G7," *Frontiers in Energy Research*, vol. 11, p. 1197030, 2023, doi: 10.3389/FENRG.2023.1197030/TEXT.

[7] IRENA, "World Energy Transitions Outlook 2023," 2023. https://www.irena.org/Digital-Report/World-Energy-Transitions-Outlook-2023.

[8] IEA, "Executive summary—Renewables 2023–analysis," 2023. https://www.iea.org/reports/renewables-2023/executive-summary.

[9] G. He, J. Lin, F. Sifuentes, X. Liu, N. Abhyankar, and A. Phadke, "Rapid cost decrease of renewables and storage accelerates the decarbonization of China's power system," *Nature Communications 2020 11:1*, vol. 11, no. 1, pp. 2486-, May 2020, doi: 10.1038/s41467-020-16184-x.

[10] M. Schmela *et al.*, "Advancements in solar technology, markets, and investments – A summary of the 2022 ISA World Solar Reports," *Solar Compass*, vol. 6, p. 100045, 2023, doi: 10.1016/J.SOLCOM.2023.100045.

[11] Alex, "Global wind report 2024," 2024. https://gwec.net/global-wind-report-2024.

[12] O. J. Ayamolowo, P. T. Manditereza, and K. Kusakana, "Exploring the gaps in renewable energy integration to grid," *Energy Reports*, vol. 6, pp. 992–999, 2020, doi: 10.1016/J.EGYR.2020.11.086.

[13] P. Purkait, M. Basu, and S. R. Nath, "Renewable Energy Integration to Electric Power Grid: Opportunities, Challenges, and Solutions," *Energy, Environment, and Sustainability*, vol. Part F2601, pp. 37–100, 2024, doi: 10.1007/978-981-97-1406-3_3/TABLES/3.
[14] L. Deguenon, D. Yamegueu, S. Moussa kadri, and A. Gomna, "Overcoming the challenges of integrating variable renewable energy to the grid: A comprehensive review of electrochemical battery storage systems," *Journal of Power Sources*, vol. 580, p. 233343, 2023, doi: 10.1016/J.JPOWSOUR.2023.233343.
[15] O. Benzohra, S. S. Echcharqaouy, F. Fraija, and D. Saifaoui, "Integrating wind energy into the power grid: Impact and solutions," *Materials Today: Proceedings*, vol. 30, pp. 987–992, 2020, doi: 10.1016/J.MATPR.2020.04.363.
[16] N. Mlilo, J. Brown, and T. Ahfock, "Impact of intermittent renewable energy generation penetration on the power system networks – A review," *Technology and Economics of Smart Grids and Sustainable Energy*, vol. 6, no. 1, pp. 25-, 2021, doi: 10.1007/S40866-021-00123-W/METRICS.
[17] M. Khalid, "Smart grids and renewable energy systems: Perspectives and grid integration challenges," *Energy Strategy Reviews*, vol. 51, p. 101299, 2024, doi: 10.1016/J.ESR.2024.101299.
[18] B. Hredzak, V. G. Agelidis, and M. Jang, "A model predictive control system for a hybrid battery-ultracapacitor power source," *IEEE Transactions on Power Electronics*, vol. 29, no. 3, pp. 1469–1479, 2014, doi: 10.1109/TPEL.2013.2262003.
[19] X. Feng, H. B. Gooi, and S. X. Chen, "Hybrid energy storage with multimode fuzzy power Allocator for PV systems," *IEEE Transactions on Sustainable Energy*, vol. 5, no. 2, pp. 389–397, 2014, doi: 10.1109/TSTE.2013.2290543.
[20] Y. Han, Y. X. Han, M. K. Lim, and M. L. Tseng, "DC microgrid with hybrid photovoltaic storage system: Control strategy optimization using improved Archimedes optimization algorithm," *Journal of Energy Storage*, vol. 118, p. 116342, 2025, doi: 10.1016/J.EST.2025.116342.
[21] F. Nawaz, E. Pashajavid, Y. Fan, and M. Batool, "Enhanced Distributed Coordinated Control Strategy for DC Microgrid Hybrid Energy Storage Systems Using Adaptive Event Triggering," *Electronics 2025, Vol. 14, Page 3303*, vol. 14, no. 16, p. 3303, 2025, doi: 10.3390/ELECTRONICS14163303.
[22] S. K. Kollimalla, A. Ukil, H. B. Gooi, U. Manandhar, and N. R. Tummuru, "Optimization of Charge/Discharge Rates of a Battery Using a Two-Stage Rate-Limit Control," *IEEE Transactions on Sustainable Energy*, vol. 8, no. 2, pp. 516–529, 2017, doi: 10.1109/TSTE.2016.2608968.
[23] B. Wang, J. Xu, R. J. Wai, and B. Cao, "Adaptive Sliding-Mode with Hysteresis Control Strategy for Simple Multimode Hybrid Energy Storage System in Electric Vehicles," *IEEE Transactions on Industrial Electronics*, vol. 64, no. 2, pp. 1404–1414, 2017, doi: 10.1109/TIE.2016.2618778.
[24] D. B. Wickramasinghe Abeywardana, B. Hredzak, and V. G. Agelidis, "A Fixed-Frequency Sliding Mode Controller for a Boost-Inverter-Based Battery-Supercapacitor Hybrid Energy Storage System," *IEEE Transactions on Power Electronics*, vol. 32, no. 1, pp. 668–680, 2017, doi: 10.1109/TPEL.2016.2527051.
[25] N. R. Tummuru, M. K. Mishra, and S. Srinivas, "Dynamic Energy Management of Renewable Grid Integrated Hybrid Energy Storage System," *IEEE Transactions on Industrial Electronics*, vol. 62, no. 12, pp. 7728–7737, 2015, doi: 10.1109/TIE.2015.2455063.
[26] F. Fracica-Rodriguez, M. Acevedo-Iles, D. Romero-Quete, W. Martinez, and C. A. Cortes, "Passivity-Based Control for Transient Power Sharing and State of Charge Restoration in a Semi-Active Supercapacitor-Battery System," *Batteries 2024, Vol. 10, Page 322*, vol. 10, no. 9, p. 322, 2024, doi: 10.3390/BATTERIES10090322.
[27] S. Abdelmalek, A. Dali, M. Bettayeb, and A. Bakdi, "A new effective robust nonlinear controller based on PSO for interleaved DC–DC boost converters for fuel cell voltage regulation," *Soft Computing*, vol. 24, no. 22, pp. 17051–17064, 2020, doi: 10.1007/S00500-020-04996-4/METRICS.
[28] M. Chen and G. A. Rincón-Mora, "Accurate electrical battery model capable of predicting runtime and I-V performance," *IEEE Transactions on Energy Conversion*, vol. 21, no. 2, pp. 504–511, 2006, doi: 10.1109/TEC.2006.874229.
[29] X. Wei, B. Zhu, and W. Xu, "Internal resistance identification in vehicle power lithium-ion battery and application in lifetime evaluation," *2009 International Conference on Measuring Technology and Mechatronics Automation, ICMTMA 2009*, vol. 3, pp. 388–392, 2009, doi: 10.1109/ICMTMA.2009.468.
[30] L. W. Yao and J. A. Aziz, "Modeling of Lithium Ion battery with nonlinear transfer resistance," *2011 IEEE Applied Power Electronics Colloquium, IAPEC 2011*, pp. 104–109, 2011, doi: 10.1109/IAPEC.2011.5779865.
[31] M. A. Albasheri, O. Bouchhida, Y. Soufi, A. Cherifi, M. A. H. Mujammal, and A. Moualdia, "Energy

management technique of hybrid energy storage system-based DC microgrid," *Journal of Energy Systems*, vol. 9, no. 1, pp. 36–51, 2025, doi: 10.30521/JES.1523522.

[32] Y. Kamagaté and H. A. Shah, "Effective dynamic energy management algorithm for grid-interactive microgrid with hybrid energy storage system," *Scientific Reports 2024 14:1*, vol. 14, no. 1, pp. 20294-, 2024, doi: 10.1038/s41598-024-70599-w.

[33] A. W. Ibrahim *et al.*, "Optimized Energy Management Strategy for an Autonomous DC Microgrid Integrating PV/Wind/Battery/Diesel-Based Hybrid PSO-GA-LADRC Through SAPF," *Technologies 2024, Vol. 12, Page 226*, vol. 12, no. 11, p. 226, 2024, doi: 10.3390/TECHNOLOGIES12110226.

[34] B. A. Taye, "Coordinated Energy Management Strategy for DC Microgrid With Hybrid Energy Storage System: A Real-Time Case Study," *Engineering Reports*, vol. 7, no. 6, p. e70241, 2025, doi: 10.1002/ENG2.70241.

[35] Q. Li, F. Zhao, L. Zhuang, Q. Wang, and C. Wu, "Research on the control strategy of DC microgrids with distributed energy storage," *Scientific Reports 2023 13:1*, vol. 13, no. 1, pp. 20622-, 2023, doi: 10.1038/s41598-023-48038-z.

[36] A. A. Saif, M. Mohamed, S. Mohammed, and M. Shafiullah, "Comparative Control Strategies and Evaluation of Hybrid Energy Storage in DC Microgrids under Dynamic Load Disturbances," *Conference Proceedings - 2025 IEEE International Conference on Energy Technologies for Future Grids, ETFG 2025*, 2025, doi: 10.1109/ETFG61999.2025.11401195.

[37] M. Zouli, S. Ghoudelbourk, A. Ouari, and D. Dib, "Influence of the external and internal parameters on the characteristics of generator PV," *AIP Conference Proceedings*, vol. 1814, no. 1, 2017, doi: 10.1063/1.4976226/842315.

[38] P. Singh and J. S. Lather, "Power management and control of a grid-independent DC microgrid with hybrid energy storage system," *Sustainable Energy Technologies and Assessments*, vol. 43, p. 100924, 2021, doi: 10.1016/J.SETA.2020.100924.

[39] C. S. G. Bhavani and D. R. Kishore, "Battery protection scheme integrated with demand side management in stand alone hybrid microgrid," *Proceedings - 2020 IEEE International Symposium on Sustainable Energy, Signal Processing and Cyber Security, iSSSC 2020*, 2020, doi: 10.1109/ISSSC50941.2020.9358847.

[40] A. T. Singo, "Photovoltaic Power Supply System with Hybrid Storage for an Energy-Autonomous Residential Building," Ph.D. dissertation, Universite Henri Poincare – Nancy 1, Nancy, France, 2010.

[41] A. Kadri, H. Marzougui, A. Aouiti, and F. Bacha, "Energy management and control strategy for a DFIG wind turbine/fuel cell hybrid system with super capacitor storage system," *Energy*, vol. 192, p. 116518, 2020, doi: 10.1016/J.ENERGY.2019.116518.

[42] S. Z. Hassan, H. Li, T. Kamal, S. Mumtaz, L. Khan, and I. Ullah, "Control and Energy Management Scheme for a PV/SC/Battery Hybrid Renwable Power System," *Science International*, vol. 28, no. 2, pp. 955–964, 2016.

[43] C. Melkia, S. Ghoudlburk, Y. Soufi, M. Maamri, and M. Bayoud, "Battery-Supercapacitor Hybrid Energy Storage Systems for Stand-Alone Photovoltaic," *Revue des Composites et des Materiaux Avances*, vol. 24, no. 5–6, pp. 265–271, 2022, doi: 10.18280/EJEE.245-605.

[44] S. Ghoudelbourk, D. Dib, B. Meghni, and M. Zouli, "Selective harmonic elimination strategy in eleven level inverter for PV system with unbalanced DC sources," *AIP Conference Proceedings*, vol. 1814, no. 1, 2017, doi: 10.1063/1.4976227/842545.